PNAS RESEARCH ARTICLE | MEDICAL SCIENCES OPEN ACCESS

A synthetic agent ameliorates polycystic kidney disease by promoting apoptosis of cystic cells through increased oxidative stress

Bogdan I. Fedeles[a,1], Rishi Bhardwaj[b], Yasunobu Ishikawa[b,2], Sakunchai Khumsubdee[a,c], Matteus Krappitz[b,3], Nina Gubina[a,d], Isabel Volpe[b], Denise C. Andrade[a,4], Parisa Westergerling[b,5], Tobias Staudner[b,6], Jake Campolo[a,7], Sally S. Liu[a], Ke Dong[b], Yiqiang Cai[b], Michael Rehman[b], Anna-Rachel Gallagher[b,8], Somsak Ruchirawat[c], Robert G. Croy[a], John M. Essigmann[a,1], Sorin V. Fedeles[b,1], and Stefan Somlo[b,1]

Edited by Ana Maria Cuervo, Albert Einstein College of Medicine, Bronx, NY; received October 9, 2023; accepted November 15, 2023

Autosomal dominant polycystic kidney disease (ADPKD) is the most common monogenic cause of chronic kidney disease and the fourth leading cause of end-stage kidney disease, accounting for over 50% of prevalent cases requiring renal replacement therapy. There is a pressing need for improved therapy for ADPKD. Recent insights into the pathophysiology of ADPKD revealed that cyst cells undergo metabolic changes that up-regulate aerobic glycolysis in lieu of mitochondrial respiration for energy production, a process that ostensibly fuels their increased proliferation. The present work leverages this metabolic disruption as a way to selectively target cyst cells for apoptosis. This small-molecule therapeutic strategy utilizes 11beta-dichloro, a repurposed DNA-damaging anti-tumor agent that induces apoptosis by exacerbating mitochondrial oxidative stress. Here, we demonstrate that 11beta-dichloro is effective in delaying cyst growth and its associated inflammatory and fibrotic events, thus preserving kidney function in perinatal and adult mouse models of ADPKD. In both models, the cyst cells with homozygous inactivation of *Pkd1* show enhanced oxidative stress following treatment with 11beta-dichloro and undergo apoptosis. Co-administration of the antioxidant vitamin E negated the therapeutic benefit of 11beta-dichloro in vivo, supporting the conclusion that oxidative stress is a key component of the mechanism of action. As a preclinical development primer, we also synthesized and tested an 11beta-dichloro derivative that cannot directly alkylate DNA, while retaining pro-oxidant features. This derivative nonetheless maintains excellent anti-cystic properties in vivo and emerges as the lead candidate for development.

mouse model | cystic disease | oxidative stress | lead optimization | apoptosis

Significance

Autosomal dominant polycystic kidney disease (ADPKD) is an incurable genetic disease affecting over 600,000 people in the United States and over 12 million people worldwide. If untreated, ADPKD leads to end-stage kidney failure in ~50% of patients by age 60, which underscores the significant need for therapies that slow down disease progression while preserving kidney function. The present work describes a therapeutic strategy for ADPKD, demonstrated here by preclinical studies in mouse models, in which cyst cells are selectively targeted for apoptosis. This effect is achieved with compounds that induce oxidative stress, to which cyst cells, owing to their disrupted metabolism, are particularly sensitive. The high efficacy of the therapeutic approach described here indicates significant potential for clinical development.

Autosomal dominant polycystic kidney disease (ADPKD), the most common monogenic cause of end-stage kidney disease, results from mutations in *PKD1* and *PKD2*, which respectively encode polycystin-1 (PC1) and polycystin-2 (PC2) (1, 2). PC1 and PC2 are expressed in the primary cilia of kidney cells and have been hypothesized to form a heteromeric receptor–channel complex, but their precise cellular functions remain incompletely understood. Initiation of kidney cyst formation in ADPKD generally occurs by a cellular recessive second hit mechanism, or by a decline in polycystin protein expression below a functional threshold; loss of polycystin function leads to an array of cellular changes including metabolic derangements in cellular respiration and energy production that accompany and promote cyst growth (2).

Indeed, the metabolic state of cystic cells in ADPKD has recently come to the fore following reports that highlight increased levels of glycolysis and decreased oxidative phosphorylation in cells lacking PC1 (2–5). These metabolic features as well as associated signaling changes are reminiscent of cancer cell metabolism (2, 3) although cyst cells lack malignant features. Subsequent studies indicated that cyst cells, akin to certain cancer cells (6, 7), harbor fundamental mitochondrial abnormalities (8–10), which manifest through altered organelle morphologies and copy number (11), decreased respiration, and a leaky electron transport chain (ETC). As a consequence, *PKD1* null cells also experience increased oxidative stress (12), likely attributable in part to diminished levels of antioxidant enzymes (13–15) and stimulated by the feed-forward regulatory loop between mitochondria and NOX4, an NADPH oxidase (16). While the excessive formation of reactive oxygen species (ROS) and associated pathophysiology is consistent with cyst cells existing in a metabolically stressed state, the underlying mechanistic connection to the absence of polycystins is not well understood (2). Nevertheless, these observations raise the possibility of therapeutic approaches that specifically target the stressed state of the cyst cells or the altered underlying metabolic and signaling pathways in cyst cells. Inhibition of glycolysis with the

[1]To whom correspondence may be addressed. Email: bogdan@mit.edu, jessig@mit.edu, sorin.fedeles@yale.edu, or stefan.somlo@yale.edu.

[2]Present address: Department of Nephrology, Aishin Memorial Hospital, Sapporo 065-0027, Japan.

[3]Present address: Nephrologisches Forschungslabor, Berlin 10117, Germany.

[4]Present address: Department of Chemistry, Saint Joseph's University, Philadelphia, PA 19131.

[5]Present address: Department of General Pediatrics, Medical Center, University of Freiburg, Freiburg 79098, Germany.

This article contains supporting information online at https://www.pnas.org/lookup/suppl/doi:10.1073/pnas.2317344121/-/DCSupplemental.

Published January 19, 2024.

chemical analog 2-deoxyglucose (17, 18), or the physiological mimic of such inhibition through a calorie-restricted diet (19, 20), leads to the amelioration of PKD in mouse models. Targeting the mitochondrial abnormalities directly either by stimulating biogenesis (11, 21), by reducing NOX4-induced oxidative stress (12), or by stimulating antioxidant enzymes through NRF2 signaling (13) leads to improved kidney function. The present work proposes an alternative strategy to mitigate disease progression in ADPKD, wherein the altered metabolic state and mitochondrial dysfunction is targeted by a selectively cytotoxic compound to specifically eliminate cyst cells.

The "11beta" family of compounds was originally developed as a collection of multi-pathway-directed anti-tumor agents featuring a chemically reactive aniline mustard tethered to a ligand for cancer-specific proteins. One compound in the family, 11beta-dichloro (CAS 865070-37-7), induces apoptosis in cancer cells and tumor xenografts (22) by a combination of mechanisms that include i) DNA damage (23) and ii) induction of oxidative stress (24). The compound is well tolerated in mice during >6 wk of daily treatment at doses of 30 mg/kg (22). We previously showed that 11beta compounds induce oxidative stress by accumulating in the mitochondria and disrupting the flow of electrons through complex I of the ETC (24), an effect independent, in the case of 11beta-dichloro, of the ability to alkylate DNA. Given the dysregulated oxidative metabolism and mitochondrial function of *Pkd1*$^{-/-}$ cells and tissues (5, 9, 10, 25), we hypothesized that 11beta compounds may exacerbate oxidative stress in *Pkd1*$^{-/-}$ cells and cause preferential apoptosis of these cyst cells thus offering a potential therapeutic approach for ameliorating polycystic disease progression in ADPKD. We explored this possibility by treating orthologous mouse models of ADPKD with 11beta-dichloro and a related compound and found that these treatments are effective in delaying cyst growth and its associated inflammatory and fibrotic events, while preserving kidney function.

Results

11Beta-Dichloro Inhibits Cystic Growth in a Neonate ADPKD Mouse Model. An established early inactivation model for ADPKD is the *Pkd1*$^{fl/fl}$; *Pkhd1-Cre* mouse in which *Pkd1* is selectively and completely inactivated in the collecting duct by postnatal day seven (P7) (26–28). The mice were treated daily by intraperitoneal (i.p.) injection with 11beta-dichloro (Fig. 1*A*) at 10 mg/kg, one third of the dose used successfully for treatment of mice bearing tumor xenografts (22). Treatment was begun at postnatal day 10 (P10), before there was significant cyst formation, and continued to postnatal day 23 (P23), at which point the cystic burden and kidney functional failure are typically advanced in this model. The mice were killed and evaluated at P24. Treatment with 11beta-dichloro resulted in significant structural improvement of PKD as evidenced by gross morphology (Fig. 1*B*; kidney panel in *SI Appendix*, Fig. S1) and quantified by reduction in two-kidney weight to body weight (KW/BW) ratio (Fig. 1*C*) and the percentage of cyst area (cystic index; Fig. 1*D*). The reduced growth of cysts was associated with improved preservation of kidney function indicated by lower levels of blood urea nitrogen (BUN;

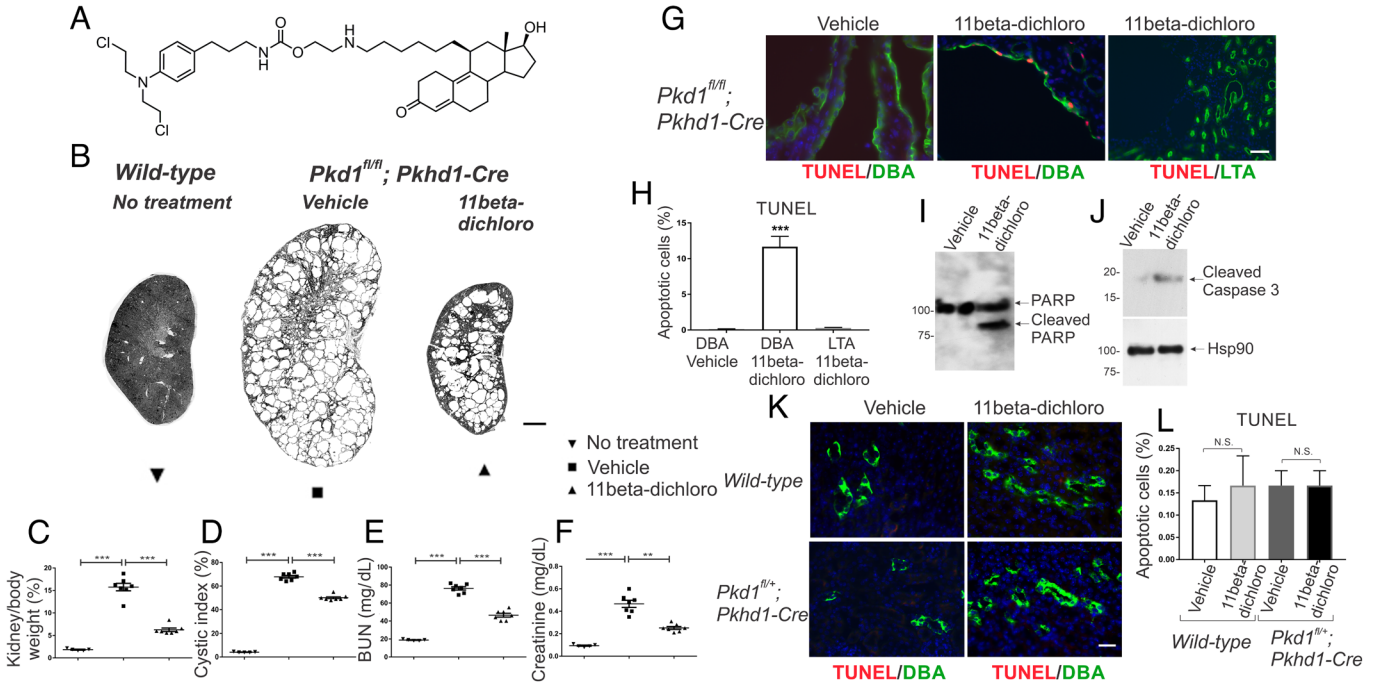

Fig. 1. 11Beta-dichloro ameliorates cystic disease in an early model of PKD by inducing apoptosis in cystic cells. (*A*) Structure of 11beta-dichloro. (*B*) Representative whole-kidney hematoxylin & eosin (H&E) scans of wild-type (*Left*), vehicle-treated (*Middle*), and 11beta-dichloro-treated (*Right*) kidneys at P24. (Scale bar, 1 mm.) Vehicle-only or 11beta-dichloro (10 mg/kg) was given i.p. daily from P10 to P23 and mice were analyzed at P24. Morphological—(*C*) two kidney/body weight ratio and (*D*) cystic index—and functional parameters—(*E*) BUN and (*F*) creatinine—show that treatment with 11beta-dichloro improved disease progression compared with vehicle-treated mice (n = 5 for WT, n = 7 for both vehicle- and 11beta-dichloro-treated cystic kidneys). (*G*) Apoptosis was evaluated in cyst lining epithelia at P24 by TUNEL staining. Compared with vehicle-treated or wild-type kidneys, 11beta-dichloro increased apoptosis in the DBA-positive (collecting duct) Cre-expressing segments. (Scale bar, 20 μm.) (*H*) Quantitation of the apoptotic index (percentage TUNEL-positive cells) in (*G*); three kidneys from three different mice per genotype and experimental condition were analyzed and >1,000 DBA-positive cells were counted for each sample. Apoptosis markers (*I*) cleaved PARP and (*J*) cleaved caspase three were increased in the 11beta-dichloro-treated vs. vehicle-treated kidneys as seen by immunoblotting. (*K*) Wild-type and *Pkd1*$^{fl/+}$;*Pkhd1-Cre* (heterozygous controls) mice were treated with 11beta-dichloro (10 mg/kg) from P10 to P23 and apoptosis was assessed via TUNEL staining. (Scale bar, 20 μm.) No increase in apoptosis was observed in the DBA-positive segments (green staining). (*L*) Quantification of the apoptotic index in (*K*), three kidneys from three different mice per genotype and kidney condition, >1,000 DBA-positive cells counted. Statistics: N.S., not significant ($P > 0.05$); $^{**}P < 0.01$; $^{***}P < 0.001$ determined by ANOVA (*C*–*F*) or *t* test (*H* and *L*). Data are plotted as mean ± SEM.

Fig. 1*E*) and serum creatinine (Fig. 1*F*) compared to vehicle-treated animals. 11Beta-dichloro was well tolerated; no significant weight loss was observed in 11beta-treated animals compared to vehicle-treated controls (*SI Appendix*, Fig. S2*A*).

In the *Pkhd1-Cre* early model of PKD, 11beta-dichloro is a potent and specific inducer of apoptosis in $Pkd1^{-/-}$ cyst cells in vivo (Fig. 1 *G–J*) while not affecting the heterozygous $Pkd1^{+/-}$ cells in normal tubules (Fig. 1 *K* and *L*). At P24, in 11beta-dichloro-treated kidneys, apoptotic (TUNEL-positive) cells were confined to collecting ducts (CD) marked by lectin *Dolichos biflorus* agglutinin (DBA), where *Pkhd1-Cre* is expressed rendering the cells $Pkd1^{-/-}$ (Fig. 1 *G* and *H*). Apoptotic cells were absent from proximal tubules (PT) marked by *Lotus tetragonolobus* agglutinin (LTA), where *Pkhd1-Cre* is not active, in 11beta-dichloro-treated kidneys, and from cystic CD of mice treated with vehicle (Fig. 1 *G* and *H*). The increased apoptosis was confirmed by the appearance of cleaved PARP (Fig. 1*I*) and cleaved caspase-3 (Fig. 1*J*) in 11beta-dichloro-treated cystic kidney lysates. No increased occurrence of apoptosis was noted in true heterozygous CD cells in treated mice (Fig. 1 *K* and *L*) indicating that the pro-apoptotic effect is dependent on the $Pkd1^{-/-}$ genotype and the heterozygous state is not sufficient to sensitize kidney tubules to apoptosis in response to 11beta-dichloro. Additionally, 11beta-dichloro had no effect on the proliferation rates (Ki67 staining) of the mutant CD cyst cells (*SI Appendix,* Fig. S2 *B* and *C*). Together, the data indicate that the therapeutic effect of the compound is based on an increased susceptibility of $Pkd1^{-/-}$ cyst cells to apoptosis in vivo that results in an altered balance of net cyst growth despite the unaltered proliferative propensity of cyst cells.

11Beta-Dichloro Inhibits Cystic Growth in an Adult ADPKD Mouse Model. An ADPKD model with slower progression more akin to human disease is the adult doxycycline-inducible $Pax8^{rtTA}$; *TetO-Cre*; $Pkd1^{fl/fl}$ ("adult Pax8") model (27). The mice receive doxycycline in the drinking water from P28 to P42 to induce *Cre* and inactivate *Pkd1* along much of the nephron. We treated this model for 12 wk beginning at P42 with three times a week i.p. injections of 11beta-dichloro (10 mg/kg body weight). When examined at 18 wk of age, 11beta-dichloro-treated mice had milder polycystic kidney disease compared to vehicle-treated mice as evidenced by gross morphology (Fig. 2*A*; kidney panel in *SI Appendix,* Fig. S3) and improvements in two-kidney weight to body weight ratio (Fig. 2*B*), cystic index, (Fig. 2*C*), BUN (Fig. 2*D*), and serum creatinine (Fig. 2*E*). No sex differences in terms of morphological response (*SI Appendix,* Fig. S4*A*) or functional response (*SI Appendix,* Fig. S4*B*) were observed. Additionally, the therapeutic regimen was well tolerated with no significant body weight loss in the treated animals vs. controls (*SI Appendix,* Fig. S4*C*), in concordance with previous mouse

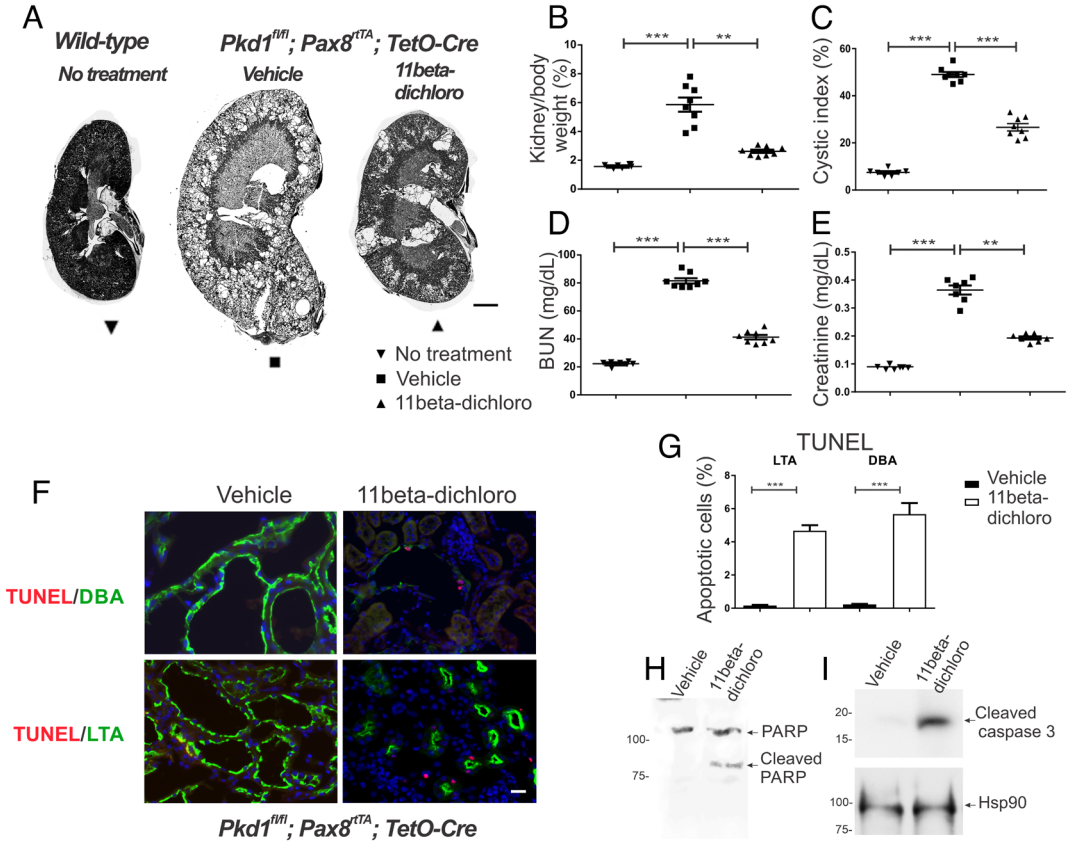

Fig. 2. 11Beta-dichloro ameliorates cystic disease in the adult Pax8 model of PKD by inducing apoptosis in cystic cells. (*A*) Representative whole kidney H&E scans of wild-type (*Left*), vehicle-treated (*Middle*), and 11beta-dichloro-treated (*Right*) kidneys. (Scale bar, 1 mm.) Morphological—(*B*) two kidney/body weight ratio and (*C*) cystic index—and functional parameters—(*D*) BUN and (*E*) creatinine—show that 11beta-dichloro treatment improved disease progression compared with vehicle-treated mice (n = 7 for wild-type and n = 8 for vehicle- and 11beta-dichloro-treated cystic groups). (*F*) Apoptosis was evaluated by TUNEL staining in cyst lining epithelia from both distal (DBA positive) and proximal (LTA positive) regions of the nephron. Compared with vehicle, 11beta-dichloro increased apoptosis in both regions of the nephron in $Pkd1^{-/-}$ animals. (Scale bar, 20 μm.) (*G*) Quantitation of the apoptotic index from (*F*), three kidneys from three mice per experimental condition, >1,000 DBA-positive or LTA-positive cells were counted for each sample. The apoptosis markers (*H*) cleaved PARP and (*I*) cleaved caspase three were increased in the 11beta-dichloro-treated vs. vehicle-treated kidneys as seen by immunoblotting. Statistics: $^{**}P < 0.01$; $^{***}P < 0.001$ determined by ANOVA (*B–E*) or *t* test (*G*). Data are plotted as mean ± SEM.

toxicity studies on 11beta-dichloro (23), which established that the dose used here (10 mg/kg) would elicit no adverse effects.

Similarly to the neonate model, the cyst lining cells in the kidneys of adult Pax8 mice treated with 11beta-dichloro showed apoptosis at substantially increased rates compared to vehicle-treated cyst lining cells, as evidenced by the increased fraction of TUNEL-positive cells in both CD and PT epithelia (Fig. 2 *F* and *G*), and increased levels of PARP cleavage (Fig. 2*H*) and cleaved caspase 3 in whole kidney extracts (Fig. 2*I*). The Pax8 transgene is expressed in both CD and PT cells (27) rendering cells in both segments *Pkd1* null and thus susceptible to enhanced apoptosis following treatment with 11beta-dichloro. Moreover, the treatment with 11beta-dichloro had no effect on cellular proliferation rate as determined by Ki67 staining, in either tissue (*SI Appendix,* Fig. S4 *D* and *E*).

11Beta-Dichloro Treatment Has Anti-Inflammatory and Anti-Fibrotic Effects in Cystic Kidneys. The therapeutic effect of 11beta-dichloro observed in both mouse models of ADPKD relies on the induction of apoptosis in cystic epithelia. However, substantial levels of cell death in an organ are commonly associated with toxicity and increased inflammation. While the mice in the above regimens do not exhibit any overt signs of systemic toxicity, owing to the use of doses of 11beta-dichloro that are significantly lower than the maximum tolerated doses previously reported (22, 23), we nonetheless explored whether the pro-apoptotic effect of the compound is locally toxic or modulates otherwise the pathophysiology of the disease.

In ADPKD, as the cysts develop in the kidneys, the tissue experiences an increased inflammatory state, which eventually stimulates fibrosis and permanent scarring (29). For example, the proinflammatory cytokine TNF-α is typically elevated in human cyst fluid; in ADPKD models, its increased levels have been associated with enhanced cyst severity (30). Both mouse models used in this study showed the same trend. We found that TNF-α protein expression is increased in $Pkd1^{-/-}$ kidney lysates in both the neonatal and the adult mouse models of ADPKD (Fig. 3 *A* and *B*). This result is corroborated by immunofluorescence (IF) studies that show a distinct increase in the TNF-α signal in the pericystic areas, in both mouse models (Fig. 3*D*). Intriguingly, the treatment with 11beta-dichloro leads to a normalization of the TNF-α levels in the cystic kidneys, as seen by western blot (WB) and IF (Fig. 3 *A*, *B*, and *D*).

One of the key transcriptional targets of TNF-α is the NLRP3 inflammasome, a protein complex responsible for activation of caspase-1, by promoting the autoproteolytic cleavage of pro-caspase-1 (31). Activated caspase-1, in turn, proteolytically activates proinflammatory cytokines IL-1β and IL-18 to their secretory forms, which further lead to sustained inflammation (31). In both our models of ADPKD, we observe increased levels of activated cleaved caspase-1 and IL-1β protein in vehicle-treated kidneys, both in tissue lysates (Fig. 3 *A* and *B*) and in the pericystic areas (Fig. 3*F*). Similarly to the changes in the TNF-α levels, the treatment with 11beta-dichloro led to a normalization of the cleaved caspase-1 and IL-1β levels in the cystic kidneys (Fig. 3 *A*, *B*, and *F*). Taken together, these observations indicate that 11beta-dichloro reduces the inflammatory effect in the kidney while promoting apoptosis of cyst cells.

An additional feature of the pathophysiology of cystic kidney diseases, including ADPKD, is the development of tubulointerstitial fibrosis linked to the activation of myofibroblasts and an increase in extra-cellular matrix deposition (29). Such changes underlie the fibrotic scarring that accompanies cystic growth, which eventually leads to permanent loss in kidney tissue and function. The mouse models employed here recapitulate these changes. Both the neonatal and adult cystic kidneys displayed an increased myofibroblast activation as seen by enhanced α-SMA (Fig. 3 *A*–*C*) and PDGFR-β levels (Fig. 3*E*). Once again, treatment with 11beta-dichloro leads to decreased levels of α-SMA and PDGFR-β in both models, which indicate a decrease of the fibrosis phenotype in conjunction with reduced cystic disease progression. Taken together, the data show that 11beta-dichloro induces selective apoptosis in $Pkd1^{-/-}$ cyst lining cells, which delays disease progression and preserves kidney function by reducing net cyst growth, without local toxicity, while also reducing the associated inflammatory and fibrotic changes that occur in ADPKD.

Oxidative Stress Underpins the Specific Toxicity of 11beta-Dichloro toward Cystic Cells. The previous mechanistic study of 11beta-dichloro toxicity in HeLa cells demonstrated the ability of the compound to localize to the mitochondrion, disrupt the flow of electrons through the ETC and induce formation of ROS (24). We investigated here whether 11beta induces ROS in $Pkd1^{-/-}$ cyst cells. *Pkhd1-Cre* cystic kidneys were harvested and stained for lipid peroxidation biomarker 4-hydroxynonenal (4-HNE), an oxidative stress-induced cellular byproduct. Recent evidence suggests that the bulk of 4-HNE in a cell is formed from the oxidation of mitochondria-specific phospholipid cardiolipin (32), and thus, it primarily reflects mitochondrial oxidative stress (33). First, we established the specificity of the anti-4-HNE antibody by treating IMCD3 cells, an established kidney epithelial cell line, with antimycin A, a known ROS stressor, or 11beta-dichloro (*SI Appendix,* Fig. S5). Both compounds elicited a positive 4-HNE signal compared with DMSO-treated cells. Next, we investigated the formation of 4-HNE in the 11beta-dichloro-treated mice. In the neonate model, 4-HNE was detected in the cyst lining cells from mice treated with 11beta-dichloro (Fig. 4*A* and *SI Appendix,* Fig. S6*A*), but only in the DBA-positive $Pkd1^{-/-}$ cyst cells, suggesting a specific induction of oxidative stress in the cystic cells. By contrast, no 4-HNE signal was detected in wild-type (PT) epithelia in the 11beta-dichloro-treated kidneys, nor in any of the vehicle-treated kidneys. Quantification of the 4-HNE signal is included in *SI Appendix,* Fig. S6*B*. The 4-HNE staining also correlated with the accumulation of genomic 7,8-dihydro-8-oxoguanine (8-oxoguanine; 8-oxoG), another established biomarker of oxidative stress (Fig. 4*B* and *SI Appendix,* Fig. S7). To bolster these observations, the transcriptional levels of a panel of oxidative stress–inducible genes (Table 1) were measured using qPCR in whole kidney extracts (Fig. 4*C*). Only cystic kidneys treated with 11beta-dichloro showed significant increases in the messenger RNA (mRNA) levels of oxidative stress–inducible genes *Cat*, *Sod1*, *Glrx*, *Gpx*, *Hmox*, *Hif1α* and *Prdx* (Table 1). 11Beta-dichloro-treated wild-type kidneys and vehicle-treated cystic kidneys showed no significant change in the expressions of these genes. The adult Pax8 model recapitulated these mechanistic insights; cystic cells treated with 11beta-dichloro displayed a higher level of 4-HNE staining (Fig. 4*D* and *SI Appendix,* Fig. S8) and 8-oxoguanine levels (Fig. 4*E* and *SI Appendix,* Fig. S7), and the mRNA levels of oxidative stress–inducible genes were significantly increased in whole kidney extracts from 11beta-dichloro-treated animals (Fig. 4*F*). To further strengthen the notion that 11beta-dichloro treatment induces oxidative stress damage to the *Pkd* null cells, malonyl-dialdehyde (MDA), another lipid peroxidation byproduct was investigated. MDA levels were markedly increased only in *Pkd* null cells treated with 11beta-dichloro, in both the neonate (*SI Appendix*, Fig. S9*A*) and the adult (*SI Appendix*, Fig. S9*B*) models of ADPKD.

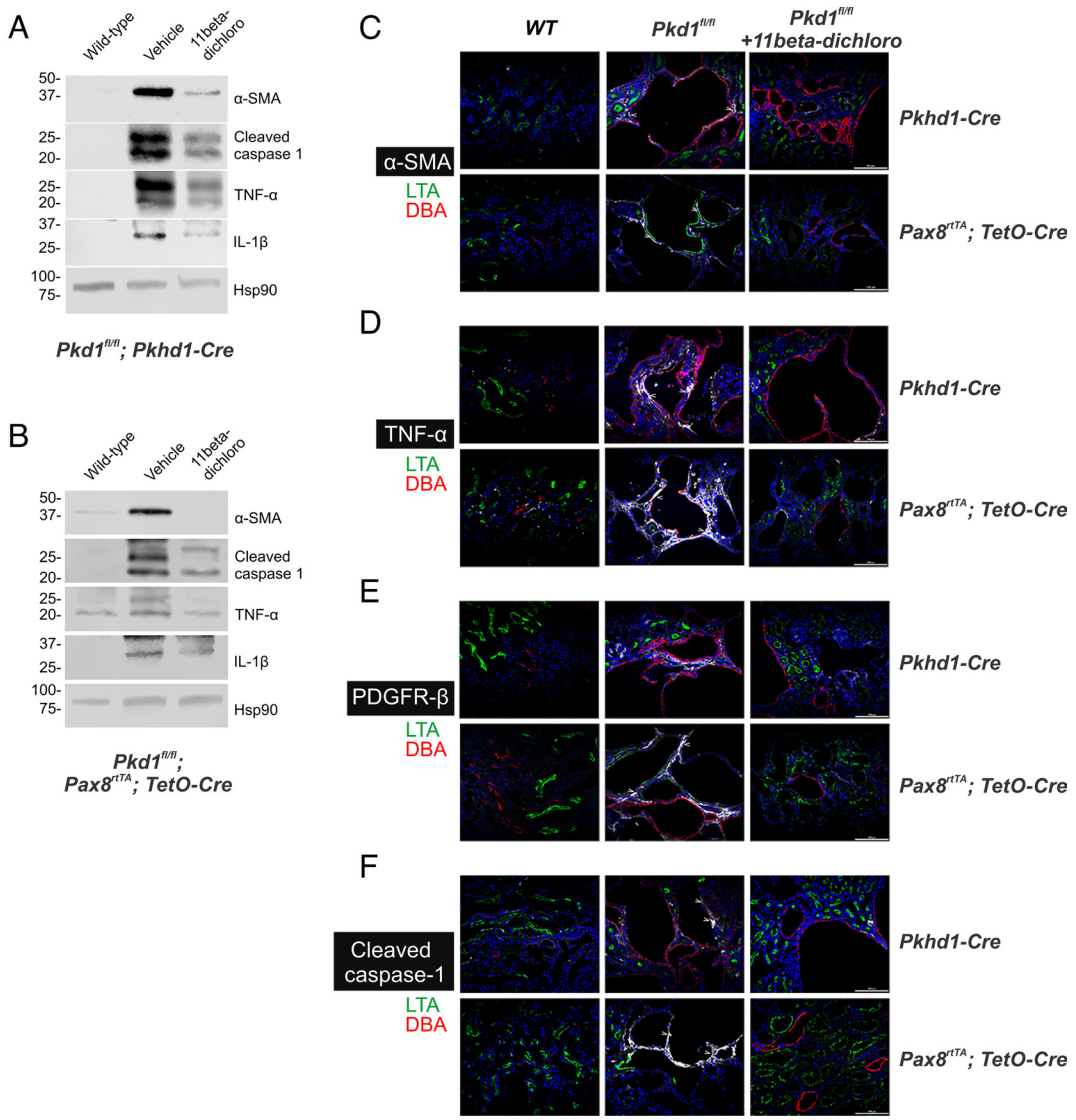

Fig. 3. Anti-inflammatory and anti-fibrotic effects of 11beta-dichloro in cystic kidneys. Changes in α-SMA expression (*A*–*C*), TNF-α (*A*, *B*, and *D*), PDGFR-β (*E*), and cleaved caspase-1 (*A*, *B*, and *F*), as a function of *Pkd1* inactivation in an early cystic model, i.e., $Pkd1^{fl/fl}$; *Pkhd1-Cre* (mice dissected at P24) or adult model, i.e., $Pkd1^{fl/fl}$, $Pax8^{rtTA}$, *TetO-Cre* (doxycycline induced inactivation of *Pkd1* from P28 to P42 and dissection at 18 wk of age), respectively. Increased levels of α-SMA, TNF-α, and cleaved caspase-1 proteins (*A* and *B*) were observed in cystic kidneys as seen via western blotting; levels were normalized after 11beta-dichloro administration. Hsp90 was used as a loading control. The findings were corroborated by immunofluorescence analysis of α-SMA (*C*), TNF-α (*D*), PDGFR-β (*E*), and cleaved caspase-1 (*F*) in cystic kidneys in the absence or presence of 11beta-dichloro treatment. Slides were co-stained with DBA (red) and LTA (green) to visualize distal and proximal sections of the nephron, respectively. Each panel in (*C*–*F*) is representative of at least one section stained from each of three separate kidneys. (Scale bar, 100 μm.)

Antioxidants Counteract the Pro-Apoptotic Effect of 11beta-Dichloro. To demonstrate that oxidative stress is an intrinsic component of the mechanism by which 11beta-dichloro targets the cyst cells for apoptosis, we repeated the 11beta-dichloro treatment of *Pkhd1-Cre* mice in the presence of the liposoluble antioxidant DL-α-tocopherol acetate (a synthetic form of vitamin E), administered in the drinking water of nursing mothers. Previous cell culture data indicated that vitamin E can buffer 11beta-dichloro-induced oxidative stress and ameliorate cell killing (24). Mice that received vitamin E concurrently with 11beta-dichloro (10 mg/kg) showed no therapeutic benefit from 11beta-dichloro (Fig. 5 *A*–*D*). The therapeutic effect of the compound on the two-kidney weight to body weight ratio (Fig. 5*B*), on the cystic index (Fig. 5*C*), and on kidney function indicated by the BUN level (Fig. 5*D*) was lost. Concomitantly, the increase in the fraction of apoptotic cells induced by 11beta-dichloro alone was absent in the presence of vitamin E (Fig. 5 *E* and *F*), and the characteristic oxidative stress biomarker, 4-HNE, was no longer present (Fig. 5*G*). Taken together, these data suggest that the induction of oxidative stress in cystic cells is a key effector step in the mechanism of action of 11beta-dichloro, a step that likely commits the cells to apoptosis. Our findings also suggest that the basis for the selectivity of the compound is the inherent sensitivity to oxidative stress of the $Pkd1^{-/-}$ cystic cells, which in turn may be attributable to their dysfunctional mitochondrial metabolism (8–12).

In both mouse models, the biomarkers analyzed (cleaved PARP, cleaved caspase 3) indicate that 11beta-dichloro is inducing apoptosis in the cyst cells. However, given the ROS production induced by the treatment, we considered whether 11beta-dichloro also induces ferroptosis. To that end, we evaluated the protein levels of ferroptosis biomarkers FTH1, SLC3A2, SLC7A11, NRF2, and KEAP1 in whole kidney lysates (*SI Appendix*, Fig. S10). The level of ferritin heavy chain 1 (FTH1) was increased in *Pkd* null kidney lysates (compared to wild-type or vehicle-only groups); however, FTH1 levels decreased after 11beta-dichloro treatment, whereas

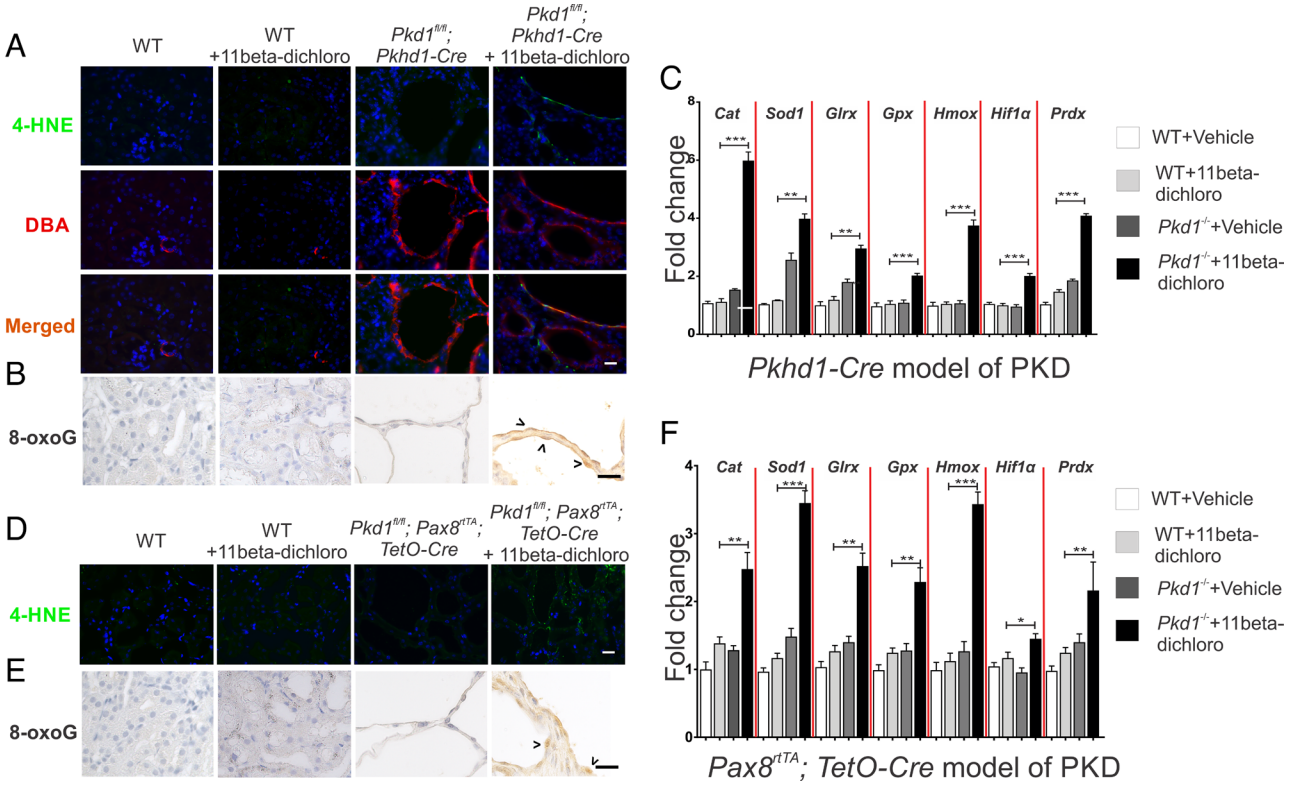

Fig. 4. 11Beta-dichloro exacerbates oxidative stress in cystic cells in both the early and adult mouse models of PKD. (*A*) In the Pkhd1-Cre model of PKD, the lipid peroxidation marker 4-HNE was used to examine the status of late ROS induction in WT and cystic epithelia in vehicle- vs. 11beta-dichloro-treated animals. The levels of 4-HNE (*Top* row) are specifically increased in the DBA-positive segments (second row) as compared with non-DBA stained tubules. Furthermore, WT mice treated with the drug from P10 to P23 did not display any overt 4-HNE signal (second column). (Scale bar, 20 μm.) (*B*) The oxidative stress biomarker 8-oxoguanine was probed in the same tissues as (*A*). Only 11beta-dichloro-treated cystic tissues displayed an increased signal. (*C*) For the early model, transcriptional levels of oxidative stress–inducible genes (Table 1) were examined via qPCR in wild-type and $Pkd1^{-/-}$ mice treated with vehicle or 11beta-dichloro. Total RNA from kidney tissue was collected at day P24; n = 5 for all groups. Only the cystic mice exposed to the drug displayed a specific activation of the indicated genes. (*D*) 4-HNE and (*E*) 8-oxoguanine staining in the adult Pax8 model of PKD. (Scale bar, 20 μm.) (*F*) For the adult Pax8 model, transcriptional levels of oxidative stress–inducible genes (Table 1) were examined via qPCR in wild-type and cystic mice treated with vehicle or 11beta-dichloro. Only the cystic mice exposed to the drug displayed a specific activation of the indicated genes. Total RNA from whole-kidney extracts was collected from mice at 5 mo of age; n = 5 for all groups. Statistics: N.S., not significant ($P > 0.05$); *$P < 0.05$; **$P < 0.01$; ***$P < 0.001$ determined by ANOVA. Data are plotted as mean ± SEM.

the other biomarkers remained unchanged. These data, together with the observation that glutathione peroxidase (GPX) mRNA levels increase upon 11beta-dichloro treatment (Fig. 4 *C* and *F*), suggest that ferroptosis is unlikely to play a major role in the cyst cell death induced by 11beta-dichloro.

Although cell line models for PKD are relatively poor mimics of the animal models, they do provide opportunities for a closer examination of mechanisms of toxicity. Dose–response curves of mouse-derived PH2 ($Pkd1^{+/-}$) and PN24 ($Pkd1^{-/-}$) kidney cells (34) show selectivity of the 11beta-dichloro compound toward null cells (*SI Appendix*, Fig. S11 *A* and *B*). The viability response was measured both by a metabolic fluorescent dye (CellTiter-Blue® assay) and by total cellular ATP levels (CellTiter-Glo® assay). The $Pkd1^{-/-}$ cells also showed higher levels of ROS after exposure to 11beta-dichloro, based on the fluorescence levels of the oxidative sensitive dye MitoSOX, a molecular probe that detects primarily mitochondrial superoxide (*SI Appendix*, Fig. S11*C*). The contribution of ROS to cytotoxicity and apoptosis was demonstrated by co-treatment with antioxidants N-acetyl-cysteine (NAC, 10 mM) and DL-α-tocopherol acetate (vitamin E, 100 μM). In both cases, lower 11beta-dichloro toxicity was observed (*SI Appendix*, Fig. S11 *D* and *E*) in both cell lines. To provide a level of generality to these results, the experiments were repeated in the porcine LLC-PK1 line and the CRISPR-derived LLC-PK1 *Pkd1* null isogenic counterpart (*Materials and Methods*). Once again, the $Pkd1^{-/-}$ cells were more sensitive to 11beta-dichloro (*SI Appendix*, Fig. S12*A*). Similarly to the mouse cells, the toxicity was alleviated by co-treating with 100 μM vitamin E (*SI Appendix*, Fig. S12*B*). Repeating the dose–response experiment in an independent, isogenic pair of mouse cell lines derived by microdissection primarily from distal tubules (*SI Appendix*, *Supplemental Methods*) yielded similar results; the *Pkd1* null cells are more sensitive to 11beta-dichloro (*SI Appendix*, Fig. S13*A*) and generate more ROS (*SI Appendix*, Fig. S13*B*) compared to their wild-type counterpart.

Table 1. Oxidative stress–inducible genes analyzed in ADPKD mouse models

Gene	Description
Cat	Catalase—breaks down hydrogen peroxide to molecular oxygen and water.
Sod1	Superoxide dismutase 1 (cytosolic)—converts superoxide to water and hydrogen peroxide
Glrx	Glutaredoxin—reduces oxidized glutathione
Gpx	Glutathione peroxidase—reduces peroxides to water using glutathione
Hmox	Heme oxygenase—catalyzes breakdown of heme
Hif1α	Hypoxia-inducible factor 1 alpha—key subunit of a master regulator of the cellular response to hypoxia
Prdx	Peroxiredoxin—thioredoxin-dependent peroxide reductase; reduces peroxides

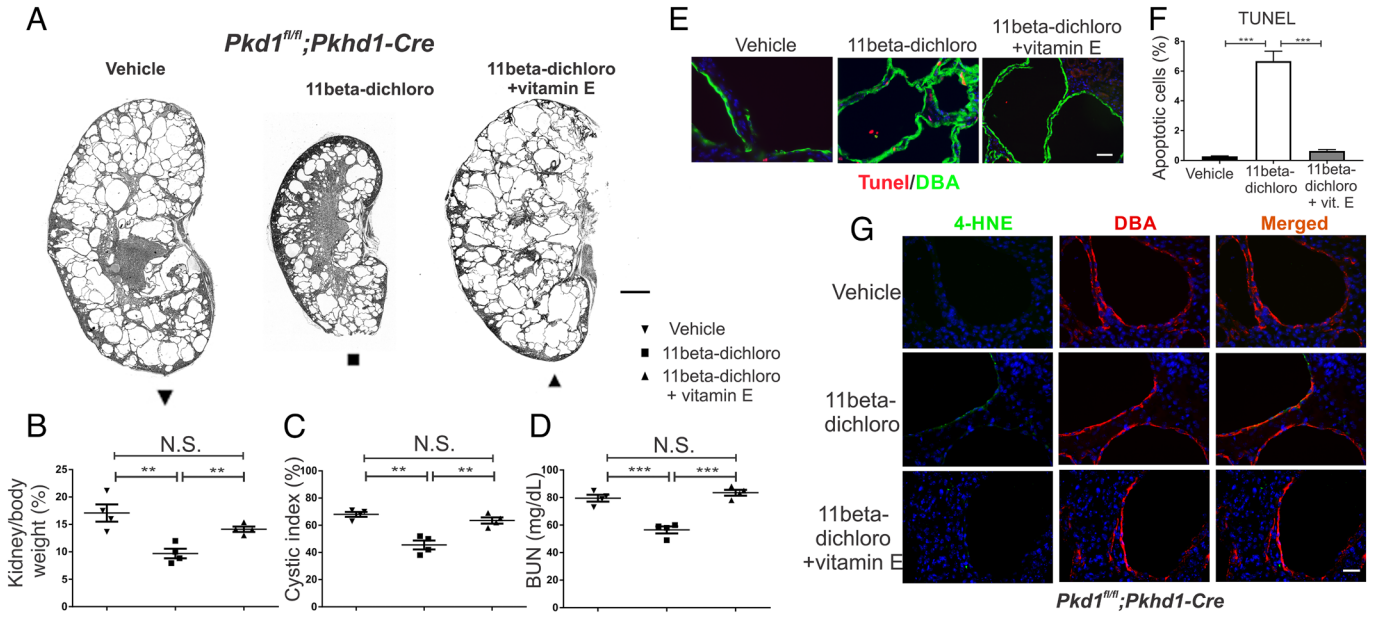

Fig. 5. Co-treatment with vitamin E abrogates the therapeutic effect of 11beta-dichloro in the early onset mouse model of ADPKD. (*A*) Representative whole kidney H&E scans of vehicle-treated (*Left*), 11beta-dichloro-treated (*Middle*), and 11beta-dichloro+vitamin E co-treated (*Right*) kidneys. (Scale bar, 1 mm.) Vehicle-only or 11beta-dichloro (10 mg/kg) was given i.p. daily from P10-P23 and mice were analyzed at P24. In addition to the 11beta-dichloro (10 mg/kg) injection, the third group received vitamin E (DL α-tocopherol acetate, 20 IU/mL) in drinking water. Morphological parameters—(*B*) two kidney/body weight ratio and (*C*) cystic index—and the functional parameter—(*D*) BUN—show that the addition of vitamin E abolishes the PKD amelioration afforded by the 11beta-dichloro treatment alone (n = 4 for all groups). (*E*) Apoptosis was evaluated by TUNEL staining in cyst lining epithelia from DBA-positive, Cre-expressing segments. The addition of vitamin E dissipates the increased apoptotic effect of 11beta-dichloro alone. (*F*) Quantitation of the apoptotic index from (*E*), three kidneys from three different mice per experimental condition, >1,000 DBA-positive cells were counted. (*G*) 4-HNE staining of tissues from (*A*), at P24. The oxidative stress induced by 11beta-dichloro alone (*Middle* row) is absent in the 11beta-dichloro+vitamin E co-treated kidneys. (Scale bar, 20 μm.) Statistics: N.S., not significant ($P > 0.05$); *$P < 0.05$; **$P < 0.01$; ***$P < 0.001$ determined by ANOVA. Data are plotted as mean ± SEM.

11Beta-Dipropyl, a Chemically Unreactive Derivative of 11beta-Dichloro, Inhibits Cyst Growth in the Early Pkhd1-Cre Mouse Model. While the therapeutic effects of 11beta-dichloro are promising, the nitrogen mustard functionality of the molecule and its ability to alkylate DNA is likely to be a hurdle in the clinical development of the compound for ADPKD. Additionally, it was important to understand the extent to which the ability of the compound to alkylate DNA (and other macromolecules) is necessary for the therapeutic effects in ADPKD mouse models. Several "defanged," chemically unreactive analogs of 11beta-dichloro have been previously prepared and tested, with findings suggesting that oxidative stress and associated toxicity is independent of the ability of the compound to alkylate DNA (24).

An isosteric derivative of 11beta-dichloro, called 11beta-dipropyl (Fig. 6*A*), was synthesized (detailed procedure in *SI Appendix*, *Supplemental Methods*) and tested in the early onset *Pkd1*$^{fl/fl}$; *Pkhd1-Cre* mouse model. The replacement of the two chlorine atoms of 11beta-dichloro with methyl groups inactivates the reactive aniline mustard and renders it unable to alkylate DNA or other biomolecules. This lack of reactivity was confirmed in two ways: 1) when incubated with the model nucleophile 4-nitrobenzylpyridine (4NBP), 11beta-dipropyl showed no measurable reactivity, in contrast with the aniline mustards 11beta-dichloro and chlorambucil (*SI Appendix*, Fig. S14); 2) gamma-H2AX staining of kidney sections treated with 11beta-dipropyl show a significantly reduced signal compared to 11beta-dichloro, indicating reduced levels of DNA damage (strand breaks) (*SI Appendix*, Fig. S15). 11Beta-dipropyl proved effective in slowing PKD development in the *Pkd1*$^{fl/fl}$; *Pkhd1-Cre* model of ADPKD at a 5 mg/kg body weight daily dose, which is half the dose used in the 11beta-dichloro experiment (Fig. 6*B*; kidney panel in *SI Appendix*, Fig. S16). No significant weight loss in treated animals was observed (*SI Appendix*, Fig. S17), suggesting low systemic toxicity. Efficacy endpoints were comparable with those observed for the treatment with 11beta-dichloro (Fig. 6 *C*–*E*). Similarly to the 11beta-dichloro treatment, the mechanism of 11beta-dipropyl involved the specific induction of apoptosis in the cystic cells (Fig. 6 *F*–*I*). Additionally, the *Pkd1*$^{-/-}$ cyst lining cells showed increased oxidative stress reflected by the accumulation of 4-HNE following treatment with 11beta-dipropyl (Fig. 6*J*). Taken together, these findings support the corollary hypothesis that the DNA alkylating activity is not necessary for the efficacy and selectivity of 11beta compounds in ADPKD, reinforcing the overarching premise that the ability of 11beta compounds to target mitochondria and induce oxidative stress are the key mechanisms by which these compounds lead to the selective apoptosis of cystic cells and improvement in preclinical outcomes in mouse models of ADPKD.

Discussion

11Beta compounds take advantage of the metabolic reprogramming of cystic cells. The upregulated glycolytic flux observed in cystic cells suggests the inability to utilize mitochondria for ATP production (3, 5). When this disrupted metabolic program is coupled with active biosynthesis for growth, which requires increased levels of reducing equivalents, such as NADPH, we speculate that the ability of the cells in the cystic epithelia to deal with redox imbalance becomes compromised. A recent study provided a mechanistic basis for the relationship between lack of PC1 protein (which leads to cystic disease) and mitochondrial dysfunction (35). Specifically, the study showed that a C-terminal peptide from PC1 stimulates by direct interaction the transmembrane mitochondrial protein NNT (NAD nucleotide transhydrogenase), a key enzyme for maintaining the mitochondrial NADPH pool. In *Pkd1*$^{-/-}$ cells, NNT activity is impaired leading to diminished

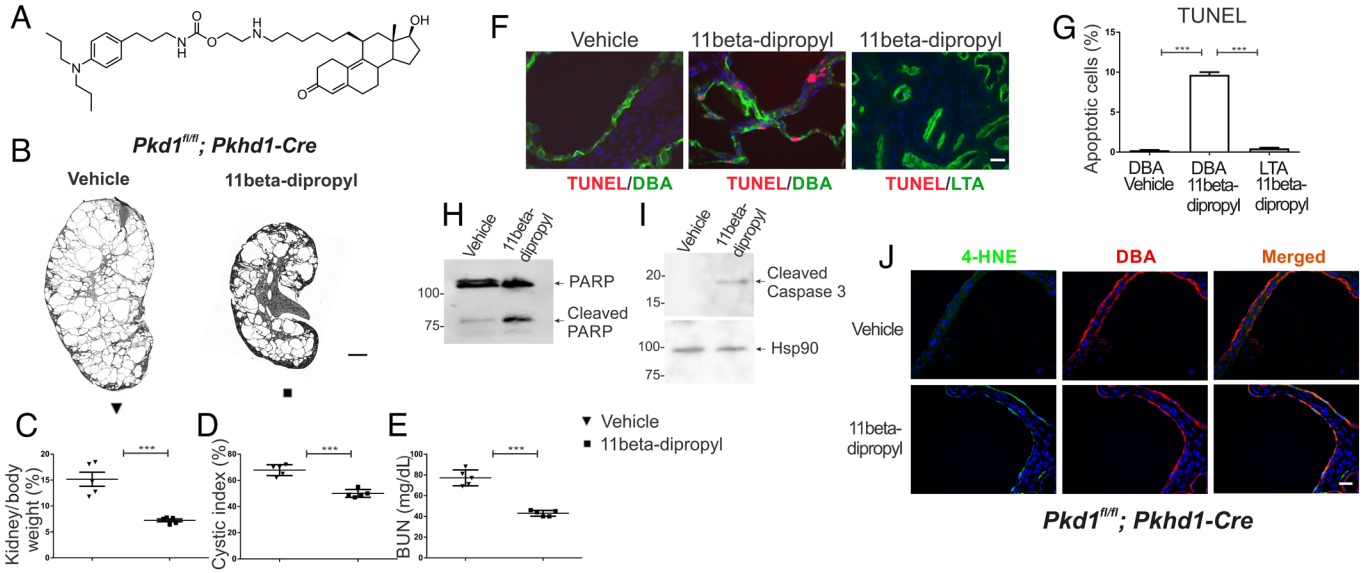

Fig. 6. The isostere 11beta-dipropyl ameliorates cystic disease in an early model of PKD by inducing apoptosis in cystic cells. (*A*) Structure of 11beta-dipropyl, an isosteric derivative of 11beta-dichloro. (*B*) Representative whole-kidney H&E scans of vehicle-treated (*Left*) and 11beta-dipropyl-treated (*Right*) kidneys. Vehicle-only or 11beta-dipropyl (5 mg/kg) was given i.p. daily from P10 to P23 and mice were analyzed at P24. (Scale bar, 1 mm.) Morphological parameters—(*C*) two kidney/body weight ratio and (*D*) cystic index—and functional parameter (*E*) BUN are all lowered in 11beta-dipropyl-treated kidneys compared to vehicle treated (n = 5 for all groups). (*F*) Apoptosis was evaluated in cyst lining epithelia by TUNEL staining. 11Beta-dipropyl increased apoptosis levels only in DBA-positive (Cre expressing) regions; vehicle-treated null cells or cells where Cre is not active (LTA-positive proximal segments) were not affected. (Scale bar, 20 μm.) (*G*) Quantitation of the apoptotic index from (*F*), three kidneys from three different mice per experimental condition, >1,000 DBA-positive cells were counted. Apoptosis markers (*H*) cleaved PARP and (*I*) cleaved caspase 3 were increased in the 11beta-dipropyl-treated vs. vehicle-treated kidneys as seen by immunoblotting. (*J*) 4-HNE staining of tissues from (*B*), at P24 indicates that 11beta-dipropyl induces oxidative stress specifically in *Pkd1*$^{-/-}$ (DBA-positive) cells. Statistics: ***$P < 0.001$ determined by ANOVA (*C*–*E*) or *t* test (*G*). Data are plotted as mean ± SEM.

NADPH levels, impaired mitochondrial metabolism, and increased oxidative stress (35). Therefore, when 11beta compounds disrupt complex I of the ETC (24), they short-circuit the already dysfunctional mitochondria, leading to such enhanced ROS production that the cyst cells are unable to tolerate. The presence of peroxidation products (4-HNE, MDA) and upregulation of many oxidative stress–inducible genes (Fig. 4) suggest a cyst cell–specific redox imbalance, due to inadequate levels of redox enzymes and cofactors (e.g., NADPH), presumably driven by both low levels of NRF2 signaling (13), and impaired NNT activity (35). We have shown previously that a key, early effect of 11beta compounds is the marked and rapid reduction in cellular NADPH level, which subsequently drives the increase in oxidative stress, with the spiraling redox imbalance eventually becoming catastrophic for the cystic cell and triggering apoptosis. These findings are corroborated by in vitro and in vivo evidence demonstrating a disease-modifying effect of ROS suppression on the apoptotic state and ultimately kidney size. In contrast with previous work (12, 13), this study provides evidence of a direct role of ROS-induced apoptosis in positively impacting polycystic kidney disease progression in relevant animal models without any impact on absolute proliferation levels. While past research has suggested that proliferation is a driver of disease progression (36), our results showcase increased apoptosis as a viable, alternative mechanism for alleviating cyst growth. In further support of this notion, we notice that the increased rates of apoptosis in the cystic tissue due to the 11beta compounds are well tolerated and without any overt local toxicity; in fact, the 11beta-dichloro treatment on the whole prevents inflammatory and fibrotic responses in the kidney (Fig. 3).

Cyst cell apoptosis has been investigated in many ADPKD models, with no clear consensus emerging regarding its involvement in disease progression (37, 38). We have not observed significant apoptosis in any *Pkd1* cystic model irrespective of timing of inactivation or tubule segment (26, 27). The only study to suggest that apoptosis may be disease modifying is that of Fan and co-workers (39), where induction of cystic epithelial cell death with Smac-mimetics delayed renal cyst growth with no effect on cell proliferation. Mechanistically, Smac-mimetics induce downregulation of cIAP1 (cellular inhibitor of apoptosis protein 1), leading to downstream activation of pro-death complex II to induce apoptosis of cystic renal epithelial cells. No assessment of ROS induction in the apoptotic phenotype was performed in that study.

Disruption of mitochondrial function as a therapeutic approach has already been established for certain cancers (40–44), and it is noteworthy in this regard that 11beta-dichloro shows good anticancer properties in animal models (22–24). Compounds that perturb the ability of mitochondria to maintain the redox homeostasis are potent inducers of apoptosis in cells experiencing oxidative stress (45, 46). The 11beta compounds expand this approach to ADPKD cells, which despite being non-cancerous, display certain metabolic features shared with cancer cells. Selective induction of apoptosis in cystic cells via exacerbating oxidative stress while sparing non-cystic cells and tissues represents a promising therapeutic paradigm for ADPKD, with 11beta family compounds holding much potential for further development into drug candidates for the clinic.

Limitations and Future Directions. The present study is a proof-of-principle study, and therefore, one limitation is the dosing regimens utilized for the animal experiments. Other regimens may further enhance the therapeutic benefit and thus warrant further investigation. Given the pro-apoptotic effect of 11beta compounds, one can envision a potential therapeutic regimen with intermittent bolus doses, where much larger doses are used but given very infrequently. Another possibility is to combine the pro-apoptotic effect of 11beta compounds with another treatment that slows down cyst cell proliferation. The 11beta-dipropyl compound, which lacks the clinically undesirable DNA-damaging functionality, has features that can guide the medicinal chemistry

efforts toward even more potent (non-mustard) compounds in the 11beta family. Taken together, both enhanced delivery options and synthetic avenues for more potent molecules represent noteworthy directions with significant potential for a clinical impact in ADPKD.

Materials and Methods

Mouse Strains and Treatment. All animal studies were conducted in accordance with Yale University Institutional Animal Care and Use Committee guidelines and procedures. The mouse strains used in the current study have previously been described: *Pkd1*$^{fl/fl}$; *Pkhd1-Cre*, *Pax8*^{rtTA}; *tetO-Cre* (27). Mice of both genders were used in this study. To account fully for biological variability, experiments utilized littermates distributed equally between vehicle-treated and drug-treated groups. The 11beta compounds were prepared in a vehicle containing cremophor®EL (Sigma):PBS:ethanol (43:30:27 by volume) and administered by i.p. injection at the doses specified. For the vitamin E treatment, nursing mothers were given DL-α-tocopherol acetate (vitamin E, SigmaMillipore) in drinking water (100 IU DL-α-tocopherol acetate/500 mL water), which corresponds to an average dose of 10 to 20 IU/kg body weight/day, starting at P7, 3 d before the treatment of the pups with 11beta-dichloro, which started at P10.

BUN and Serum Creatinine Measurement. At the terminal end points indicated, blood samples were collected from mice and sent for BUN and serum creatinine measurements at the Yale Mouse Phenotype core facility.

Immunofluorescent Staining. Mice were anesthetized via i.p. injection of ketamine/xylazine. One kidney was snap frozen, and the other kidney was fixed with 4% paraformaldehyde (PBS) via cardiac perfusion prior to histological analysis. Sections (5 to 7 μm) were prepared for immunohistochemical studies according to standard procedures (34). Images were obtained using a Nikon Eclipse TE2000-U microscope under the control of MetaMorph software (Universal Imaging) (34). The following antibodies and lectins were used: fluorescein-labeled *Lotus tetragonolobus* lectin (LTL, Vector Laboratories); fluorescein-labeled DBA (Vector Laboratories); rabbit anti-Ki67 (Sigma), rabbit anti-4-HNE (Abcam), anti 8-OHdG (8-oxoguanine, 8-oxoG)(Abcam), mouse anti-cleaved caspase-1 (p20) (Adipogen International), mouse anti-TNF-α (Santa Cruz Biotechnology), rabbit anti-α-SMA (Abcam), rabbit anti-PDGF-β (Abcam).

Proliferation analysis was performed by immunohistochemistry using rabbit anti-Ki67 monoclonal antibody. Apoptosis analysis was carried out by TUNEL staining according to the manufacturer's instructions (Roche). Sections were also stained with DAPI and DBA and the number of Ki67- or TUNEL-positive nuclei in at least 1,000 DBA-positive nuclei per kidney were counted to determine the rates for proliferation and apoptosis, respectively.

RNA Isolation, RT-PCR, and Quantitative RT-PCR. Total RNA was isolated from kidney tissue using Qiazol reagent (Qiagen) and used for cDNA synthesis using a High Capacity cDNA Reverse Transcription Kit (Applied Biosystems). Quantitative RT-PCR was performed using SYBR green fluorescent reagent and analyzed by an Mx3000 PCR System (Stratagene).

Protein Preparation and Immunoblot Analysis. Frozen whole kidneys were homogenized in ice-cold NET buffer (150 mM NaCl, 50 mM Tris-HCl, pH 7.4, 1 mM EDTA, and 0.1% Triton X-100) containing Complete EDTA-free protease inhibitor cocktail tablets (Roche) and PhosSTOP phosphatase inhibitor cocktail tablets (Roche) using a 2-mL Dounce homogenizer (Wheaton). Protein concentrations were measured with Protein Assay Dye Reagent Concentrate (Bio-Rad). Proteins were electrophoretically separated on 4.5% sodium dodecyl-sulphate polyacrylamide gels and transferred to a PVDF membrane (PerkinElmer). Membranes were sequentially incubated with primary antibodies overnight at 4 °C after 1 h of blocking with 5% milk. The following primary antibodies were used: rabbit anti-PARP (Cell signaling), rabbit anti-caspase 3 (Cell Signaling), mouse anti-cleaved caspase-1 (p20) (Adipogen International), mouse anti-TNF-α (Santa Cruz Biotechnology), and rabbit anti-α-SMA (Abcam). Secondary antibodies included anti-mouse/anti-rabbit HRP-conjugated antibodies (1:10,000) (Jackson ImmunoResearch Laboratories) which were incubated with the membrane for 1 h at RT. Western Lightning Plus-ECL (PerkinElmer) or SuperSignal West Femto Chemiluminescent Substrate (Thermo Scientific) was used for chemiluminescence detection.

Immunohistochemistry. Kidney sections were deparaffinated in xylene (3 × 10 min), hydrated in ethanol (3 × 10 min) followed by blocking in methanol:hydrogen peroxide (10%) for 30 min at room temperature. EDTA antigen retrieval was followed by rinsing in 0.05% Tween 20 in phosphate-buffered saline (3 × 5 min; 1 × PBS, pH 7.4) and blocked with 1% BSA (American Bio) prior to adding the primary antibody and incubated overnight at 4 °C. The kidney sections were rinsed with 0.05% Tween 20 in PBS (3 × 5 min), incubated for 30 min at room temperature with secondary antibody (goat anti-rat horseradish peroxidase; 1:500; Invitrogen, A10549) and finally developed with 3-3′-diaminobenzidine (Vector labs, Sk-4100). The sections were counterstained with Harris hematoxylin (1:10; SIGMA, GH5380) for 10 s, washed in distilled water (10 min) and dehydrated as follows, ethanol (3 × 5 min) and xylene (3 × 5 min) before being mounted using sub-x clearing media (Leica microsystems Inc., 3801741).

Power Calculations. STPLAN v4.5 was used to determine the group sizes for all experiments. Detecting 50% improvement in kidney/body weight or BUN with >95% power at $P < 0.05$ requires a minimum of 5 mice per group.

Cell Lines. PH2 (*Pkd1*$^{+/-}$) and PN24 (*Pkd1*$^{-/-}$) murine cell lines were produced in house as previously described (34). Briefly, both lines were derived from a single Pkd1$^{fl/-}$ murine line obtained from the H-2Kb-tsA58 mouse (ImmortoMouse, Charles River). These cells carry an SV40 transgene that confers unlimited growth potential at a permissive temperature (33 °C) in the presence of γ-interferon. PN24 (*Pkd1*$^{-/-}$) were produced from *Pkd1*$^{fl/-}$ cells by transient transfection with a plasmid expressing the Cre recombinase. This method ensures that the control and experimental cell lines are genetically identical to each other except for their genotype at *Pkd1* (34).

Generation of Pkd1 Knockout LLC-PK1 Cell Line using CRISPR-Cas9 Double-Nick Method. The *LLC-PK1* cell line was from ATCC (Catalog # CL-101). LLC-PK1 *Pkd1*$^{-/-}$ was generated in house using the CRISPR-Cas9 technique as follows. Guide RNA sequences were designed to target near the exon 2 and exon 3 of pig Pkd1 genomic DNA, in order to maximize the effect of gene disruption. *Pkd1* sgRNAs were designed with CRISPR Design Tool http://crispr.mit.edu/ (sgRNAs ACAACTCTGTCAGCGCTGAG and TGGCATTCCACGGGGTGAAC for *Pkd1* exon 2 editing, sgRNAs GGGGGTTCGACCCGGTTGGA and CCAGGGACATAAGCAACAAC for Pkd1 exon 3 editing). Two pairs of 20-nt sgRNAs for *Pkd1* knockout were cloned into pGL3-U6-sgRNA-PGK-Hygromycin plasmid which was obtained from the modified pGL3-U6-sgRNA-PGK-puromycin plasmid (Plasmid #51133, Addgene). Cas9 D10A plasmid (CMV-hspCas9(D10A)-T2A-Puro, Cat#: CASLV100PA-1, SBI), pMDLg/pRRE, pRSV-Rev, and pMD2.G were transfected into the HEK 293T cell line with Lipofectamine 2000 (Invitrogen) to generate Cas9 D10A lentivirus. Cas9 D10A lentivirus was transfected into *LLC-PK1* cell lines and the infected cells were selected with puromycin to obtain the stable Cas9 D10A *LLC-PK1* cell lines. pGL3-U6-sgRNA-PGK-Hygromycin with *Pkd1*-specific sgRNAs were transfected into Cas9 D10A LLC-PK1 stable cells. Individual cells were transferred into 96-well plates after selection with hygromycin and puromycin. The cells were reseeded and cultured in the plates in duplicate after expansion for 2 to 3 wk with antibiotics. The cells from the plates were collected and digested overnight in lysis buffer. PCR products were amplified from the extracted and purified genomic DNA of the different clones. Final *Pkd1* knockout *LLC-PK1* cell lines carrying frameshift insertion-deletions (indels) in exon 2 and exon 3 sequences of *Pkd1* genomic DNA were determined by sequencing of the PCR products. *Pkd1* knockout *LLC-PK1* cell lines were further confirmed with western blot using *polycystin-1* antibody (7E12, sc-130554, Santa Cruz Biotechnology, Inc.).

Cell Culture. PH2 and PN24 cell lines were maintained and passaged in DMEM/F12 media (Gibco #10565018), supplemented with 2% FBS (Hyclone), 1X ITS-G (Gibco #41400045), penn-strep (Gibco #15140163), T3 hormone (2 nM, Sigma Aldrich T5516), and mouse γ-interferon (5 U/mL, Sigma I4777) in a humidified incubator at 33 °C, supplemented with 5% CO2. Cells used for experiments did not exceed 15 passages. For dose–response experiments, cells were switched to 37 °C, in DMEM media (Gibco) supplemented with GlutaMAX (Gibco) and 10% FBS, for 5 d. These conditions inactivate the SV40 expression and allow the cells to differentiate. Cells were seeded in 96-well black/clear bottom culture plates (Corning #3904) at a density of 10,000 cells per well and allowed to attach overnight. 11Beta compounds (dissolved in DMSO) were diluted in media and added to the cells at the indicated concentrations (final DMSO concentration not

exceeding 0.1%). For co-treatments with antioxidants, N-acetyl-cysteine (Sigma-Aldrich) or DL-α-tocopherol acetate (Sigma-Aldrich) was added to the media at 10 mM and 100 μM final concentrations, respectively. Cells were then incubated for 24 h. Viability was measured using either the CellTiter-Blue® (Promega) or CellTiter-Glo® (Promega) assays, according to the manufacturer's instructions. Fluorescence readings at ex/em 555/585 for the CellTiter-Blue® assay, and luminescence readings for the CellTiter-Glo® assay were performed on a SpectraMax® M3 spectrophotometer (Molecular Devices). The CellTiter-Blue® assay uses the ability of cells to convert the redox dye resazurin to the fluorescent product resorufin as a proxy for viability. CellTiter-Glo® assay uses a chemiluminescence reaction to measure the total amount of ATP released upon cell lysis, which correlates with the number of viable cells.

LLC-PK1 cell lines were maintained and passaged in DMEM media (Gibco) supplemented with penn-strep and 5% FBS. Dose–response viability assays were carried out as described above, using the CellTiter-Glo® assay (Promega).

Synthesis of 11beta-Dipropyl. The synthetic route used for preparation of 11beta-dipropyl follows a convergent synthesis developed for the preparation of 11beta-dichloro analogs (22). The penultimate synthetic step involves addition of the 4-(N, N-bis-substituted aminophenyl)-propylamine followed by a final deprotection step. The 4-(N, N-bis-propylaminophenyl)-propylamine building block has been prepared in 4 steps with a 60 to 70% overall yield starting with 6-(6-aminophenyl)-butyric acid. Details are provided in *SI Appendix*, *Supplemental Methods*.

Primers Sequences for qPCR.

Gene	Forward primer	Reverse primer
Sod1	CCAGTGCAGGACCTCATTTT	CACCTTTGCCCAAGTCATCT
Cat	GGCATCAAAAACTTGCCTGT	GGGAAAGTTTCTGCCTCCT
Gpx	TGCATCGTCACCAACGTGGC	TAGCCGGCTGCAAACTCCTT
Glrx	AACAACACCAGTGCGATTCA	ATCTGCTTCAGCCGAGTCAT
Hmox	CACGCATATACCCGCTACCT	TGTGCTTGACCTCAGGTGTC
Hif1α	GGTTCCAGCAGACCCAGTTA	GATGCCTTAGCAGTGGTCGT
Prdx	GCTCTTGCTCACGCAGTCAT	GTCCTCAGCATGGTCGCTAA

Data, Materials, and Software Availability. All study data are included in the article and/or *SI Appendix*.

ACKNOWLEDGMENTS. We thank Lonnette Diggs in the George M. O'Brien Kidney Center at Yale (P30 DK079310) for BUN and creatinine measurements. T.S. and P.W. were recipients of a TRENAL scholarship, a thematic network grant of the German Academic Exchange Service (Deutscher Akademischer Austauschdienst, DAAD). This work was supported by a PKD foundation grant (198G14a to A.-–R.G), a Department of Defense Peer Reviewed Medical Research Program collaborative award (W81XWH-15-1-0365 to S.S. and J.M.E.), and the NIH grants R01-CA080024 (to J.M.E.), R01-CA26731 (to J.M.E.) and the National Institutes of Environmental Health Sciences center grant P30-ES002109 to the Center for Environmental Health Sciences at MIT, which provided bioanalytical support.

Author affiliations: [a]Departments of Biological Engineering, Chemistry and Center for Environmental Health Sciences, Massachusetts Institute of Technology, Cambridge, MA 02139; [b]Department of Internal Medicine, Section of Nephrology, Yale School of Medicine, New Haven, CT 06510; [c]Laboratory of Medicinal Chemistry, Chulabhorn Research Institute, Bangkok 10210, Thailand; and [d]Institute of Theoretical and Experimental Biophysics, Russian Academy of Sciences, Pushchino 142290, Russia

Author contributions: B.I.F., R.B., Y.I., S.K., N.G., S.R., R.G.C., J.M.E., S.V.F., and S.S. designed research; B.I.F., R.B., Y.I., S.K., M.K., N.G., I.V., P.W., T.S., J.C., S.S.L., M.R., S.R., R.G.C., and S.V.F. performed research; S.K., N.G., D.C.A., P.W., T.S., K.D., Y.C., M.R., A.-R.G., R.G.C., and S.V.F. contributed new reagents/analytic tools; B.I.F., R.B., Y.I., S.K., M.K., N.G., R.G.C., S.V.F., and S.S. analyzed data; B.I.F., S.R., J.M.E., S.V.F., and S.S. supervised research; and B.I.F., J.M.E., S.V.F., and S.S. wrote the paper.

Competing interest statement: The patent US9982009 was granted to B.I.F., R.G.C., J.M.E., S.V.F., and S.S., and assigned to Massachusetts Institute of Technology and Yale University. The patent covers the use of the 11beta-dipropyl and related compounds as therapeutics for polycystic kidney disease and polycystic liver disease. All other authors declare no competing interests.

This article is a PNAS Direct Submission.

[6]Present address: Institute of Cellular and Molecular Physiology, Friedrich-Alexander University of Erlangen-Nürnberg, Erlangen 91054, Germany.

[7]Present address: Atlas AI, Palo Alto, CA 94301.

[8]Present address: 4:59 NewCo., Boston MA 02116.

1. E. Cornec-Le Gall, A. Alam, R. D. Perrone, Autosomal dominant polycystic kidney disease. *Lancet* **393**, 919–935 (2019).
2. L. F. Menezes, G. G. Germino, The pathobiology of polycystic kidney disease from a metabolic viewpoint. *Nat. Rev. Nephrol.* **15**, 735–749 (2019).
3. I. Rowe *et al.*, Defective glucose metabolism in polycystic kidney disease identifies a new therapeutic strategy. *Nat. Med.* **19**, 488–493 (2013).
4. I. Rowe, A. Boletta, Defective metabolism in polycystic kidney disease: Potential for therapy and open questions. *Nephrol. Dial. Transplant.* **29**, 1480–1486 (2014).
5. V. Padovano, C. Podrini, A. Boletta, M. J. Caplan, Metabolism and mitochondria in polycystic kidney disease research and therapy. *Nat. Rev. Nephrol.* **14**, 678–687 (2018), 10.1038/s41581-018-0051-1.
6. E. Reznik *et al.*, Mitochondrial DNA copy number variation across human cancers. *Elife* **5**, e10769 (2016).
7. F. Weinberg *et al.*, Mitochondrial metabolism and ROS generation are essential for Kras-mediated tumorigenicity. *Proc. Natl. Acad. Sci. U.S.A.* **107**, 8788–8793 (2010).
8. H. Pellegrini *et al.*, Cleavage fragments of the C-terminal tail of polycystin-1 are regulated by oxidative stress and induce mitochondrial dysfunction. *J. Biol. Chem.* **299**, 105158 (2023).
9. C.-C. Lin *et al.*, A cleavage product of polycystin-1 is a mitochondrial matrix protein that affects mitochondria morphology and function when heterologously expressed. *Sci. Rep.* **8**, 2743 (2018).
10. Y. Ishimoto *et al.*, Mitochondrial abnormality facilitates cyst formation in autosomal dominant polycystic kidney disease. *Mol. Cell. Biol.* **37**, e00337-17 (2017).
11. L. Cassina, M. Chiaravalli, A. Boletta, Increased mitochondrial fragmentation in polycystic kidney disease acts as a modifier of disease progression. *FASEB J.* **34**, 6493–6507 (2020), 10.1096/fj.201901739RR.
12. A. S. Kahveci *et al.*, Oxidative stress and mitochondrial abnormalities contribute to decreased endothelial nitric oxide synthase expression and renal disease progression in early experimental polycystic kidney disease. *Int. J. Mol. Sci.* **21**, 1994 (2020).
13. Y. Lu *et al.*, Activation of NRF2 ameliorates oxidative stress and cystogenesis in autosomal dominant polycystic kidney disease. *Sci. Transl. Med.* **12**, eaba3613 (2020).
14. K. L. Nowak *et al.*, Vascular dysfunction, oxidative stress, and inflammation in autosomal dominant polycystic kidney disease. *Clin. J. Am. Soc. Nephrol.* **13**, 1493–1501 (2018).
15. R. L. Maser, D. Vassmer, B. S. Magenheimer, J. P. Calvet, Oxidant stress and reduced antioxidant enzyme protection in polycystic kidney disease. *J. Am. Soc. Nephrol.* **13**, 991–999 (2002).
16. S. Dikalov, Cross talk between mitochondria and NADPH oxidases. *Free Radic. Biol. Med.* **51**, 1289–1301 (2011).
17. M. Chiaravalli *et al.*, 2-Deoxy-d-glucose ameliorates PKD progression. *J. Am. Soc. Nephrol.* **27**, 1958–1969 (2016).
18. R. Magistroni, A. Boletta, Defective glycolysis and the use of 2-deoxy-D-glucose in polycystic kidney disease: From animal models to humans. *J. Nephrol.* **30**, 511–519 (2017).
19. K. R. Kipp, M. Rezaei, L. Lin, E. C. Dewey, T. Weimbs, A mild reduction of food intake slows disease progression in an orthologous mouse model of polycystic kidney disease. *Am. J. Physiol. Renal Physiol.* **310**, F726–F731 (2016).
20. G. Warner *et al.*, Food restriction ameliorates the development of polycystic kidney disease. *J. Am. Soc. Nephrol.* **27**, 1437–1447 (2016).
21. S. Hajarnis *et al.*, microRNA-17 family promotes polycystic kidney disease progression through modulation of mitochondrial metabolism. *Nat. Commun.* **8**, 14395 (2017).
22. J. C. Marquis *et al.*, Disruption of gene expression and induction of apoptosis in prostate cancer cells by a DNA-damaging agent tethered to an androgen receptor ligand. *Chem. Biol.* **12**, 779–787 (2005).
23. S. M. Hillier *et al.*, DNA adducts formed by a novel antitumor agent 11beta-dichloro in vitro and in vivo. *Mol. Cancer Ther.* **5**, 977–984 (2006).
24. B. I. Fedeles *et al.*, Chemical genetics analysis of an aniline mustard anticancer agent reveals complex I of the electron transport chain as a target. *J. Biol. Chem.* **286**, 33910–33920 (2011).
25. V. Padovano *et al.*, The polycystins are modulated by cellular oxygen-sensing pathways and regulate mitochondrial function. *Mol. Biol. Cell* **28**, 261–269 (2017).
26. S. V. Fedeles *et al.*, A genetic interaction network of five genes for human polycystic kidney and liver diseases defines polycystin-1 as the central determinant of cyst formation. *Nat. Genet.* **43**, 639–647 (2011).
27. M. Ma, X. Tian, P. Igarashi, G. J. Pazour, S. Somlo, Loss of cilia suppresses cyst growth in genetic models of autosomal dominant polycystic kidney disease. *Nat. Genet.* **45**, 1004–1012 (2013).
28. Y. Cao *et al.*, Chemical modifier screen identifies HDAC inhibitors as suppressors of PKD models. *Proc. Natl. Acad. Sci. U.S.A.* **106**, 21819–21824 (2009).
29. C. J. Song, K. A. Zimmerman, S. J. Henke, B. K. Yoder, Inflammation and fibrosis in polycystic kidney disease. *Results Probl. Cell Differ.* **60**, 323–344 (2017).
30. J. X. Zhou, L. X. Fan, X. Li, J. P. Calvet, X. Li, TNFα signaling regulates cystic epithelial cell proliferation through Akt/mTOR and ERK/MAPK/Cdk2 mediated Id2 signaling. *PLoS One* **10**, e0131043 (2015).
31. M. D. McGeough *et al.*, TNF regulates transcription of NLRP3 inflammasome components and inflammatory molecules in cryopyrinopathies. *J. Clin. Invest.* **127**, 4488–4497 (2017).
32. W. Liu, N. A. Porter, C. Schneider, A. R. Brash, H. Yin, Formation of 4-hydroxynonenal from cardiolipin oxidation: Intramolecular peroxyl radical addition and decomposition. *Free Radic. Biol. Med.* **50**, 166–178 (2011).
33. M. Xiao, H. Zhong, L. Xia, Y. Tao, H. Yin, Pathophysiology of mitochondrial lipid oxidation: Role of 4-hydroxynonenal (4-HNE) and other bioactive lipids in mitochondria. *Free Radic. Biol. Med.* **111**, 316–327 (2017).
34. S. Shibazaki *et al.*, Cyst formation and activation of the extracellular regulated kinase pathway after kidney specific inactivation of Pkd1. *Hum. Mol. Genet.* **17**, 1505–1516 (2008).

35. L. Onuchic *et al.*, The C-terminal tail of polycystin-1 suppresses cystic disease in a mitochondrial enzyme-dependent fashion. *Nat. Commun.* **14**, 1790 (2023).
36. S. V. Fedeles, A.-R. Gallagher, S. Somlo, Polycystin-1: A master regulator of intersecting cystic pathways. *Trends Mol. Med.* **20**, 251–260 (2014).
37. E. Agborbesong, L. X. Li, L. Li, X. Li, Molecular mechanisms of epigenetic regulation, inflammation, and cell death in ADPKD. *Front. Mol. Biosci.* **9**, 922428 (2022).
38. J. X. Zhou, X. Li, "Apoptosis in polycystic kidney disease: From pathogenesis to treatment" in *Polycystic Kidney Disease*, X. Li, Ed. (Codon Publications, 2015) (6 October 2021).
39. L. X. Fan *et al.*, Smac-mimetic-induced epithelial cell death reduces the growth of renal cysts. *J. Am. Soc. Nephrol.* **24**, 2010–2022 (2013).
40. A. P. Nayak, A. Kapur, L. Barroilhet, M. S. Patankar, Oxidative phosphorylation: A target for novel therapeutic strategies against ovarian cancer. *Cancers (Basel)* **10**, 337 (2018).
41. G. Battogtokh, Y.-Y. Cho, J. Y. Lee, H. S. Lee, H. C. Kang, Mitochondrial-targeting anticancer agent conjugates and nanocarrier systems for cancer treatment. *Front. Pharmacol.* **9**, 922 (2018).
42. S. Pustylnikov, F. Costabile, S. Beghi, A. Facciabene, Targeting mitochondria in cancer: Current concepts and immunotherapy approaches. *Transl. Res.* **202**, 35–51 (2018).
43. T. Dickerson, C. E. Jauregui, Y. Teng, Friend or foe? Mitochondria as a pharmacological target in cancer treatment. *Future Med. Chem.* **9**, 2197–2210 (2017).
44. S. Vyas, E. Zaganjor, M. C. Haigis, Mitochondria and cancer. *Cell* **166**, 555–566 (2016).
45. J.-Y. Tang *et al.*, Oxidative stress-modulating drugs have preferential anticancer effects-involving the regulation of apoptosis, DNA damage, endoplasmic reticulum stress, autophagy, metabolism, and migration. *Semin. Cancer Biol.* **58**, 109–117 (2019).
46. M. L. Circu, T. Y. Aw, Reactive oxygen species, cellular redox systems, and apoptosis. *Free Radic. Biol. Med.* **48**, 749–762 (2010).